Effect of Four-α-Helix Bundle Cavity Size on Volatile Anesthetic Binding Energetics†

Gavin A. Manderson, Stuart J. Michalsky, and Jonas S. Johansson*

Department of Anesthesia and the Johnson Research Foundation, University of Pennsylvania, Philadelphia, Pennsylvania 19104

Received April 18, 2003; Revised Manuscript Received July 24, 2003

ABSTRACT: Currently, it is thought that inhalational anesthetics cause anesthesia by binding to ligand-gated ion channels. This is being investigated using four-α-helix bundles, small water-soluble analogues of the transmembrane domains of the "natural" receptor proteins. The study presented here specifically investigates how multiple alanine-to-valine substitutions (which each decrease the volume of the internal binding cavity by 38 Å^3) affect structure, stability, and anesthetic binding affinity of the four-α-helix bundles. Structure remains essentially unchanged when up to four alanine residues are changed to valine. However, stability increases as the number of these substitutions is increased. Anesthetic binding affinities are also affected. Halothane binds to the four-α-helix bundle variants with 0, 1, and 2 substitutions with equivalent affinities but binds to the variants with 3 and 4 more tightly. The same order of binding affinities was observed for chloroform, although for a particular variant, chloroform was bound less tightly. The observed differences in binding affintes may be explained in terms of a modulation of van der Waals and hydrophobic interactions between ligand and receptor. These, in turn, could result from increased four-α-helix bundle binding cavity hydrophobicity, a decrease in cavity size, or improved ligand/receptor shape complementarity.

Inhalational anesthetics are currently thought to induce anesthesia by binding to membrane-bound proteins (*1*, *2*). Although the specific receptors have yet to be identified, ligand-gated ion channels and neurotransmitter receptors of the CNS[1] are likely candidates. These are generally large oligomeric membrane-bound assemblies, where the polypeptide chain of each subunit of the functional receptor or pore makes several passes through the membrane. Few crystal structures of such receptors are currently available, secondary to technical limitations. An exception, however, is that for KcsA, a K^+ channel from *Streptomyces lividans* (*3*), where the ion-conducting pore is a four-α-helix bundle and thus may offer some insight into the structure of anesthetic receptors.

The oligomeric structure and membrane-bound nature of KcsA illustrates the obstacles that would be associated with studying the binding of inhalational anesthetics to ligand-gated ion channels and other membrane proteins. For example, detergents needed to maintain protein solubility have to be carefully selected so that the affinities of subunits for one another are not altered, which would compromise the integrity of the native α-helix bundles. More importantly, the presence of detergents may alter the affinity of anesthetics for their protein receptors.

To circumvent these potential problems, which could ultimately result in ambiguous experimental findings, small water-soluble synthetic α-helix bundles are being used as model systems to study anesthetic binding (*4*−*8*). In recent years, studies with four-α-helix bundles have met with considerable success (*4*, *5*, *7*, *8*). A K_d of 710 μM was reported for the binding of halothane to $(A\alpha_2)_2$ (*5*). This suggests a binding interaction that would be only slightly weaker than that of halothane with its in vivo human "receptors" (EC_{50} value of 250 μM; *1*). A four-α-helix bundle model system therefore has considerable relevance to in vivo systems. In addition to KcsA, this motif is found in α-catenin (*9*), the focal adhesion targeting (FAT) domain of focal adhesion kinase (*10*), and ion channels formed through tetramerization of the 20-mer peptide alamethicin (*11*).

The structure of the four-α-helix bundle used in the present study, $(A\alpha_2\text{-L38M})_2$, is depicted in Figure 1. The polypeptide chain, N-terminus to C-terminus, Leu-Lys-Lys-Leu-Arg-Glu-Glu-Ala-Ala-Lys-Leu-Phe-Glu-Glu-Trp-Lys-Lys-Leu-Ala-Glu-Glu-Ala-Ala-Lys-Leu-Leu-Glu-Gly-Gly-Gly-Gly-Gly-Gly-Gly-Gly-Glu-Leu-Met-Lys-Leu-Cys-Glu-Glu-Ala-Ala-Lys-Lys-Ala-Glu-Glu-Leu-Phe-Lys-Leu-Ala-Glu-Glu-Arg-Leu-Lys-Lys-Leu, was designed to assume a helix−turn−helix structure in aqueous solution, which then dimerizes in an antiparallel manner to form the four-α-helix bundle. Each $A\alpha_2$-L38M monomer has 62 residues, 27 of which are in each of the two α-helix-forming regions, separated by an eight-residue glycine linker region. The α-helices each have 7.5 turns, and the interior cavity of the bundle is hydrophobic (*7*). Tryptophan 15 is at heptad position a in the center of helices I and III; the side chain points into the hydrophobic interior of the four-α-helix bundle. The inclusion of a tryptophan in the sequence means that four-α-helix bundle

† Supported by NIH Grant GM55876.

* Corresponding author. Mailing address: 319C John Morgan Building, University of Pennsylvania, 3620 Hamilton Walk, Philadelphia, PA 19104. Telephone: 215-349-5472. Fax: 215-349-5078. E-mail: JohanssJ@uphs.upenn.edu.

[1] Abbreviations: CNS, central nervous system; Fmoc, 9-fluorenylmethoxycarbonyl; NMP, *N*-methylpyrrolidone; DCM, dichloromethane; TFA, 2,2,2-trifluoroacetic acid; CD, circular dichroism; Gdn-HCl, guanidine hydrochloride; $[Gdn\text{-}HCl]_{mid}$, guanidine hydrochloride concentration at which half of the four-α-helix bundle is unfolded; NATA, *N*-acetyltryptophanamide.

10.1021/bi034623b CCC: $25.00
Published on Web 09/05/2003

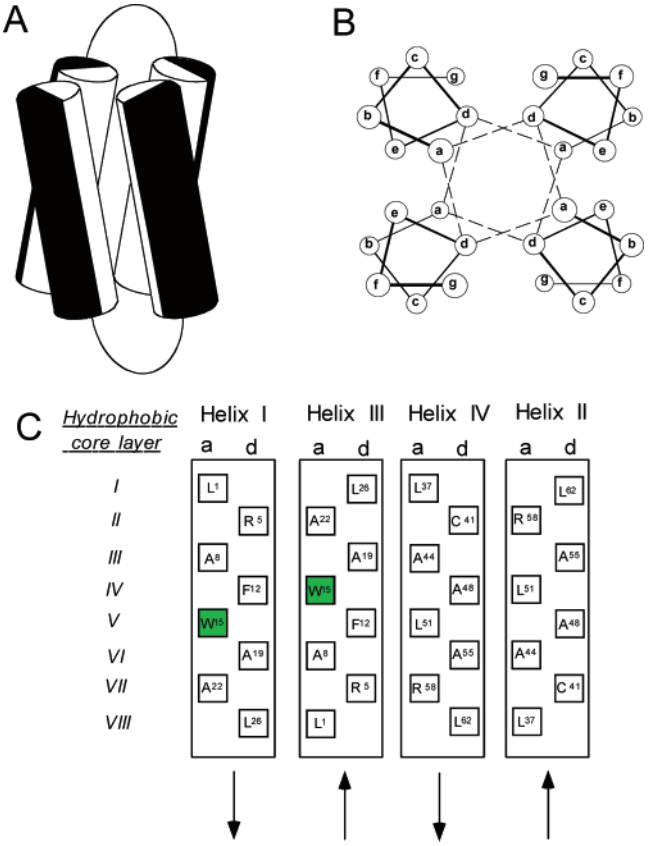

FIGURE 1: Representations of the structure of $(A\alpha_2\text{-L38M})_2$ and variants. (A) Cartoon. Four-α-helix bundles were formed as a consequence of the antiparallel association of two polypeptide chains, which each fold to assume an α-helix−turn−α-helix topology in solution. The turn is formed in an eight glycine linker region. The N-termini are at the top left-hand and bottom right-hand ends of the front and rear polypeptide chains, respectively. (B) α-Helical wheel depiction, where the letters denote the heptad positions. (C) Directionality of the α-helices of $(A\alpha_2\text{-L38M})_2$. Helices I and IV are antiparallel to helices II and III. The side chains at heptad positions a and d only are shown, and the amino acid position from the N-terminus is given. Tryptophan 15 is shaded.

concentrations can be determined spectrophotometrically and fluorescence spectroscopy can be used to follow structural change, since the emission λ_{max} of this side chain is dependent on solvent polarity (*12*). More importantly, it has been shown earlier that anesthetics bind within the hydrophobic cavity and interact with the side chain of Trp^{15} (*7*, *8*, *13*). Results from a photolabeling study (*7*) demonstrated that the majority of a radioactive ligand was covalently bound to the side chain of Trp^{15}. Anesthetic binding can thus be easily followed by measuring changes in the extent of fluorescence quenching.

The four-α-helix bundle $(A\alpha_2\text{-L38M})_2$ was chosen as the starting point for the present study because it has a higher affinity for the anesthetic halothane than $(A\alpha_2)_2$ (*7*). By changing Leu^{38} to Met^{38}, halothane binding affinity was increased 3.5-fold (to $K_d = 200\ \mu M$). This improvement was attributed to better shape complementarity in the hydrophobic core of the four-α-helix bundle. The side chain of methionine, being unbranched, is more flexible than that of leucine. Additionally, the highly polarizable sulfur atom of methionine probably plays a role in improving the strength of the dipole interactions between the anesthetic and the side chain of residue 38.

In a second substitution study, Trp^{15} of $(A\alpha_2\text{-L38M})_2$ was changed to Tyr^{15}. This substitution provided important information regarding the nature of the interaction between the anesthetic and the aromatic residue at position 15 (*8*). A 6-fold decrease in halothane binding affinity occurred as a consequence of the W15Y substitution. This implicates dipole−aromatic quadrupole interactions as being important in anesthetic binding.

The studies described above, aimed at refining the structure of $(A\alpha_2)_2$ for anesthetic binding, are continued in the present study. Ultimately, the structure of the hydrophobic cavity of a four-α-helix bundle that binds anesthetics tightly could be used to develop the criteria necessary to successfully identify the in vivo anesthetic receptors. In the present study, up to four alanine-to-valine substitutions were made in the $(A\alpha_2\text{-L38M})_2$ sequence. Figure 1 shows that all of these were made at either heptad positions a or d and close to Trp^{15} in hydrophobic core layers III and VI; the intention was to increase the hydrophobicity and decrease the size of the internal binding cavity in the region where the anesthetic is bound. The original $(A\alpha_2\text{-L38M})_2$ and variants were then characterized to determine whether structure and stability had been altered and whether anesthetic binding affinity had been improved as a consequence of the introduction of alanine-to-valine substitutions.

Alanine-to-valine substitutions may affect anesthetic binding affinity in a number of ways. First, the overall hydrophobicity of the internal cavity will be increased, potentially improving the compatibility of the binding site with the lipophilic anesthetics. Second, these substitutions may decrease the size of the internal cavity, permitting a tighter fit of the anesthetic in the binding site. Third, the specific shape of the valine side chain and position of placement in the internal cavity may improve the shape complementarity between anesthetic and binding site. To corroborate the findings for halothane, the binding of another anesthetic, chloroform, to the four-α-helix bundles was investigated.

With respect to four-α-helix bundle structure and stability, it was expected that unfolding would become more unfavorable as a consequence of such substitutions due to increased hydrophobicity in the core. Whether the stepwise increase in the number of alanine to valine substitutions led to a corresponding stepwise increase in stability was also examined.

MATERIALS AND METHODS

Materials. 9-Fluorenylmethoxycarbonyl- (Fmoc-) protected amino acids and all reagents required for peptide synthesis were purchased from Perkin-Elmer Applied Biosystems (Foster City, CA). Acetonitrile was from Fisher Scientific (Pittsburgh, PA). Ethanedithiol was obtained from Fluka (Buchs, Switzerland). Halothane (2-bromo-2-chloro-1,1,1-trifluoroethane) was from Halocarbon Laboratories (Hackensack, NJ). The thymol preservative present in this commercial sample was removed by alumina column chromatography (*14*). All other chemicals were of reagent grade or better and were obtained from the Sigma Aldrich Chemical Co. (St. Louis, MO).

Peptide Synthesis and Purification. The peptides were assembled as the C-terminal carboxyamides on a 0.25 mM scale using (Fmoc) amino acids and Fmoc-2,4-dimethoxy-

benzhydrylamide resin on an Applied Biosystems Model 433A (Perkin Elmer, Foster City, CA) solid-phase peptide synthesizer. Standard coupling conditions with 2-(1*H*-benzotriazol-1-yl)-1,1,3,3-tetramethyluronium hexafluorophosphate, 1-hydroxybenzotriazole, and *N*,*N*-diisopropylethylamine in *N*-methylpyrrolidone (NMP) and a 4-fold molar excess of amino acid was used throughout. The resin was washed with NMP and dichloromethane (DCM), and N-terminal acetylation was performed with acetic anhydride/pyridine (1:1 by volume). The acetylated peptides were again washed with NMP and DCM and cleaved from the resin, and the protecting groups were removed for 240 min in 2,2,2-trifluoroacetic acid (TFA)−ethanedithiol−water (90:8:2 by volume). Reversed-phase C_{18} high-performance liquid chromatography with aqueous acetonitrile gradients [45% (v/v) to 70% (v/v) over 60 min] containing 0.1% (v/v) TFA was used to purify crude peptides to homogeneity. Peptide identities were confirmed with laser desorption mass spectrometry.

In all, five four-α-helix bundles were synthesized: the original $(A\alpha_2\text{-L38M})_2$ of ref *7* and the following variants: $(A\alpha_2\text{-L38M/A8V})_2$, $(A\alpha_2\text{-L38M/A8V/A19V})_2$, $(A\alpha_2\text{-L38M/A8V/A19V/A44V})_2$, and $(A\alpha_2\text{-L38M/A8V/A19V/A44V/A55V})_2$.

Circular Dichroism Spectroscopy. The spectra of 10 μM solutions of dimeric four-α-helix bundles were recorded on a model 62 DS spectropolarimeter (Aviv, Lakewood, NJ) using 2 mm path-length quartz cells, a bandwidth of 1.0 nm, a scan step of 0.5 nm, and a time constant of 3.0 s. The buffer was 10 mM sodium phosphate, pH 7.0. The cell holder was maintained at 25.0 ± 0.1 °C.

Fluorescence Spectroscopy. Tryptophan fluorescence measurements were made on 2 μM solutions of dimeric four-α-helix bundles in a tightly stoppered 1 cm path-length quartz cell using a Shimadzu Model RF 5301 fluorescence spectrophotometer (Columbia, MD). Samples were excited at 280 nm (1.5 nm excitation bandwidth), and the emission spectrum was recorded over the appropriate wavelength range (emission bandwidth 5.0 nm) at a scan step of 0.2 nm. Correction of emission λ_{max} data for instrument response was not necessary because the experimentally determined λ_{max} of standard compounds (*15*) were found to be within 1.0 nm of their published values. The cell holder temperature was 25.0 ± 0.1 °C. For guanidine hydrochloride- (Gdn-HCl-) induced denaturation studies (see below) the buffer was 10 mM sodium phosphate, pH 7.0. Other buffer systems are described in the appropriate sections.

Denaturation Studies. Denaturation of the four-α-helix bundles was examined using two techniques: fluorescence spectroscopy, monitoring tryptophan emission λ_{max}, and circular dichroism (CD) spectroscopy, monitoring mean residue ellipticity at 222 nm ($[\theta]_{222}$) as described earlier (*5*). The measured tryptophan emission λ_{max} and $[\theta]_{222}$ were plotted as a function of [Gdn-HCl] and fit to an equation describing the unfolding of a dimeric single domain protein (*16*), using a nonlinear least-squares routine:

$$\text{fraction folded} = [[\exp(\Delta G^{H_2O} + m[\text{denaturant}])]/RT]/[4P(1 + (8P/(\exp(\Delta G^{H_2O} + m[\text{denaturant}])/RT)) - 1)^{1/2}] \quad (1)$$

where ΔG^{H_2O} is the conformational stability of the protein, m is the slope of the unfolding transition, and P is the molar monomer concentration of the protein. To confirm repeatability, fluorescence emission λ_{max} data for each variant were collected on two separate occasions.

Renaturation of $(A\alpha_2\text{-}L38M)_2$. An examination of the reversibility of four-α-helix bundle denaturation was made using the original $(A\alpha_2\text{-L38M})_2$ structure. Aliquots from a stock solution of $(A\alpha_2\text{-L38M})_2$ in 5.0 M Gdn-HCl were diluted to 2 μM $(A\alpha_2\text{-L38M})_2$ using various volumes of both buffer and stock 8.0 M Gdn-HCl solution. In using both buffer and Gdn-HCl for dilutions, the 2 μM $(A\alpha_2\text{-L38M})_2$ could be prepared at a range of final chaotrope concentrations between 5.0 and 0.2 M. Data were treated as described above. It was assumed that the behavior observed for $(A\alpha_2\text{-L38M})_2$ would be representative of that of all the four-α-helix bundles examined in the present study.

Tryptophan Fluorescence Quenching. End-Point Titration of $(A\alpha_2\text{-}L38M)_2$ *and Variants with* $LaCl_3$. Solutions of $(A\alpha_2\text{-L38M})_2$ and variants at 2 μM in 10 mM HEPES buffer were each titrated with 200 mM $LaCl_3$, in the same buffer, until no further decrease in tryptophan emission intensity was observed. Fluorescence emission spectra were collected as described above. A HEPES buffer system was used because $LaPO_4$ is insoluble. The titration data for each variant are displayed as a Stern−Volmer plot (F_0/F vs $[LaCl_3]$), where F_0 is the unquenched fluorescence intensity and F is the fluorescence intensity at a given $LaCl_3$ concentration. The plots were then fit, using a nonlinear least-squares routine, to a modified Stern−Volmer equation, which takes into account solvent-accessible and solvent-inaccessible populations of tryptophan side chains (*17*):

$$F_0/F = (1 + K_{SV}\alpha[La^{3+}])/(1 + K_{SV}[La^{3+}]) \quad (2)$$

where α is the fraction of solvent-inaccessible tryptophan and K_{SV} is $1/K_d$.

Ligand Binding Measurements. The binding of the anesthetics halothane and chloroform to the four-α-helix bundles was measured by following the change in tryptophan fluorescence emission intensity as the ligand-free species was titrated with increasing amounts of ligand-equilibrated species. The four-α-helix bundles were prepared in 20 mM sodium phosphate buffer, 130 mM NaCl, pH 7.0, to a final concentration of 2 μM. The ligand-equilibrated four-α-helix bundles were prepared by introducing volumes of halothane or chloroform into gastight Hamilton syringes (Reno, NV), containing 2 μM four-α-helix bundles, to final concentrations of 10 mM halothane and 35 mM chloroform, and mixing for 1 h. The intermediate anesthetic concentrations were obtained by mixing apo- and anesthetic-equilibrated samples to give the final concentrations indicated in the figures. The extent of quenching (Q) observed is a function of the maximum possible quenching (Q_{max}) at infinite anesthetic concentration and the affinity of the anesthetic for the binding site on each four-α-helix bundle (K_d; *4*, *5*, *7*) close to the tryptophan side chain:

$$Q = (Q_{max}[\text{anesthetic}])/(K_d + [\text{anesthetic}]) \quad (3)$$

The data for each four-α-helix bundle was displayed as a Stern−Volmer plot (F_0/F vs [anesthetic]). Each plot had been

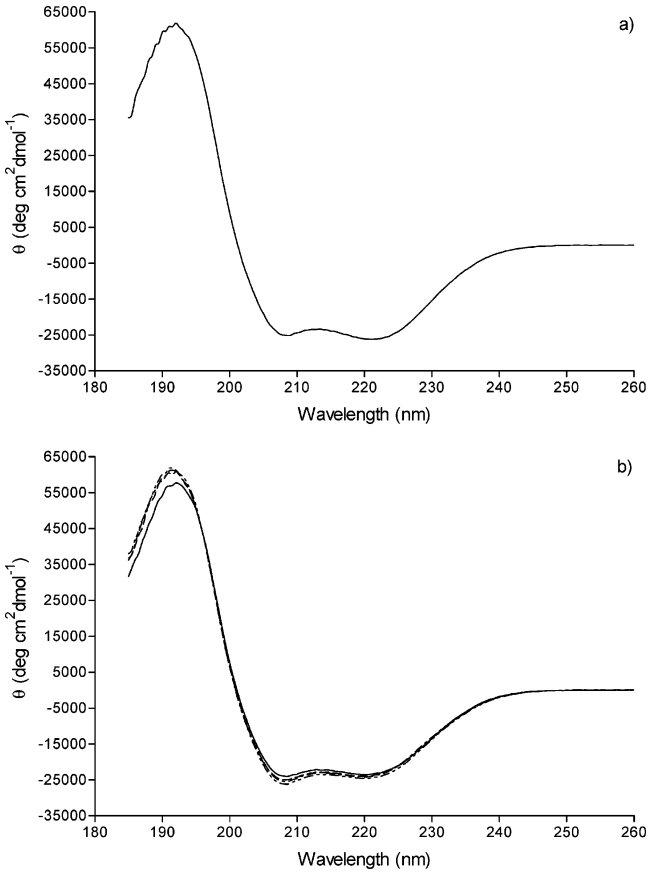

FIGURE 2: Far-UV CD spectra of $(A\alpha_2\text{-}L38M)_2$ and variants at 10 μM under nondenaturing conditions (10 mM sodium phosphate buffer, pH 7.0). Panels: (a) $(A\alpha_2\text{-}L38M)_2$; (b) $(A\alpha_2\text{-}L38M)_2$, (—); $(A\alpha_2\text{-}L38M/A8V)_2$, (---); $(A\alpha_2\text{-}L38M/A8V/A19V)_2$, (— —); $(A\alpha_2\text{-}L38M/A8V/A19V/A44V)_2$, (— - —); $(A\alpha_2\text{-}L38M/A8V/A19V/A44V/A55V)_2$, (— -- —).

previously corrected for dynamic quenching of tryptophan fluorescence by anesthetic. The Stern−Volmer function for anesthetic-induced quenching of tryptophan fluorescence from $(A\alpha_2\text{-}L38M)_2$ in 5.0 M Gdn-HCl was subtracted from plots prepared using data collected in the absence of Gdn-HCl. Values for K_{SV}, the slope of the corrected plots, were then determined. In calculating K_{SV} in this manner, it was assumed that all quenching was static, occurring as a consequence of the retention of the quencher/ligand in close proximity to the fluorophore. To confirm repeatability, triplicate measurements on each variant with each anesthetic were made on two separate occasions.

RESULTS

Structure of $(A\alpha_2\text{-}L38M)_2$ and Variants under Nondenaturing Conditions. From far-UV CD spectroscopy it is evident that $(A\alpha_2\text{-}L38M)_2$ (Figure 2a) and variants (Figure 2b) contain predominantly α-helix in 10 mM sodium phosphate buffer, pH 7.0. The spectra are very similar to that of poly(L-lysine) in an all-α-helical conformation (*18*). In theory, a polypeptide chain of 62 residues, where 54 residues are predicted to exist in an α-helical conformation, should give a $[\theta]_{222}$ of −35563 deg cm^2 dmol^{-1} (*19*). Using this value, the percentage of α-helical structure in $(A\alpha_2\text{-}L38M)_2$ and variants was calculated using experimentally determined $[\theta]_{222}$ values (Table 1). The values are all similar to those obtained in earlier studies for proteins of similar structure: $(A\alpha_2)_2$ (64.7% α-helix; *7*), the three helix bundles α_3D (68.5%; *20*) and α_3-1 (80.5%; *5*), deoxymyoglobin (73.0%; *21*), and erythrocyte spectrin (76.0%; *22*). Substituting up to four alanines for valine does not have an appreciable effect on the proportion of α-helix in $(A\alpha_2\text{-}L38M)_2$ (Table 1), even though the relative probability (P_α) that valine will occur in an α-helical conformation (P_α = 1.09) is lower than that for alanine (P_α = 1.60; *23*).

Tryptophan fluorescence emission λ_{max} values were also used to gain insight into the structures of $(A\alpha_2\text{-}L38M)_2$ and variants under nondenaturing conditions (Table 1). The emission λ_{max} for tryptophan increases with increasing solvent polarity, from 308 nm (in azurin) to 352 nm (in glucagon; *12*). Therefore, the values for $(A\alpha_2\text{-}L38M)_2$ and variants, which are between 321 and 326 nm (Table 1), suggest that the tryptophan side chains of these four-α-helix-bundles are sequestered in hydrophobic environments. This is consistent with a three-dimensional structure where the side chain of tryptophan points into the internal hydrophobic cavity of the four-α-helix bundles.

To further examine the environments of the tryptophan side chain of $(A\alpha_2\text{-}L38M)_2$ and variants under nondenaturing conditions, a fluorescence quenching study using La^{3+} (*24*) was conducted. The four-α-helix bundles, at a concentration of 2 μM, were titrated with La^{3+}, and the results are shown in Figure 3a. In using La^{3+}, however, the buffer had to be changed to 10 mM HEPES, pH 7.0, due to the insolubility of $LaPO_4$. Lanthanum(III) was selected as a quenching agent because it is highly charged and should not enter into the hydrophobic interior of the four-α-helix bundles to any appreciable extent. Therefore, La^{3+} should be more suited to discriminating between solvent-accessible and buried tryptophan side chains than neutral polar quenchers such as acrylamide. The experimental data (Figure 3a) confirm this assumption. All of the Stern−Volmer plots show a pronounced curvature toward the *x* axis. This indicates two populations of tryptophan side chains (*12*), one of which is inaccessible to La^{3+}. The observed downward curvature is also consistent with a predominantly dynamic quenching mechanism; the La^{3+} does not appear to interact in a specific manner with the indole ring of tryptophan (*12*). The possible occurrence of some through-space quenching of buried tryptophan side chains is acknowledged. However, the curvature of the Stern−Volmer plots (Figure 3a) makes this unlikely. Among the five variants examined here, $(A\alpha_2\text{-}L38M/A8V/A19V/A44V/A55V)_2$ showed the most pronounced quenching (Figure 3b), suggesting a greatest extent of tryptophan side chain solvent exposure.

Far-UV CD data can give an indication of whether the α-helices of an α-helix bundle, or coiled coil, interact. This will be true if the ratio $[\theta]_{222}/[\theta]_{208}$ is approximately 1.0 (*25*, *26*). The $\theta_{222}/\theta_{208}$ values for $(A\alpha_2\text{-}L38M)_2$ and variants (Table 1) fall within the range 0.93−0.96, showing little dependence on the number of alanine-to-valine substitutions. These ratios are thus consistent with the notion that the α-helices of $(A\alpha_2\text{-}L38M)_2$ and variants interact to form a four-α-helix bundle.

Denaturation Studies. The conformational stability of $(A\alpha_2\text{-}L38M)_2$ and variants was examined by following the change in tryptophan fluorescence emission λ_{max} and $[\theta]_{222}$ as a function of Gdn-HCl concentration. There is an appreciable increase in tryptophan emission λ_{max} for $(A\alpha_2\text{-}$

Table 1: Spectral and Thermodynamic Properties of $(A\alpha_2\text{-L38M})_2$ Four-α-Helix Bundles

four-α-helix bundle	solution M_r	fluorescence emission λ_{max} (nm)[b]	$[\theta]_{222}$ (deg cm^2 dmol^{-1}) [% α-helix]	$[\theta]_{222}/[\theta]_{208}$	$[Gdn]_{mid}$ (M)[a]	ΔG^{H_2O} (kcal/mol)[a]	m [kcal/(mol M)][a]
$(A\alpha_2\text{-L38M})_2$	13772.2	325	−24000 [73.4]	0.96	3.0 ± 0.1 *2.4 ± 0.1*	−15.2 ± 0. 6 *−11.2 ± 0.*5	2.8 ± 0.2 *1.5 ± 0.2*
$(A\alpha_2\text{-L38M/Val})_2$	13828.4	326	−23000 [77.8]	0.96	3.3 ± 0.1 *3.0 ± 0.1*	−14.8 ± 0.6 *−16.2 ± 0.6*	2.5 ± 0.2 *2.9 ± 0.2*
$(A\alpha_2\text{-L38M/2Val})_2$	13884.4	321	−23500 [74.0]	0.94	4.0 ± 0.3 *3.8 ± 0.5*	−18.9 ± 1.4 *−23.2 ± 3.1*	3.0 ± 0.4 *4.0 ± 0.8*
$(A\alpha_2\text{-L38M/3Val})_2$	13940.6	321	−23600 [75.2]	0.93	4.2 ± 0.2 *4.2 ± 0.4*	−18.2 ± 0.7 *−21.2 ± 2.1*	2.6 ± 0.2 *3.5 ± 0.5*
$(A\alpha_2\text{-L38M/4Val})_2$	13996.6	323	−24200 [77.1]	0.93	4.9 ± 0.2 *4.8 ± 0.4*	−18.6 ± 0.9 *−24.4 ± 2.3*	2.4 ± 0.2 *3.4 ± 0.5*

[a] Roman type for thermodynamic parameters determined from CD data. Italic type for analogous parameters determined from fluorescence data. [b] The wavelength calibration of the instrument was checked as described in the Materials and Methods section.

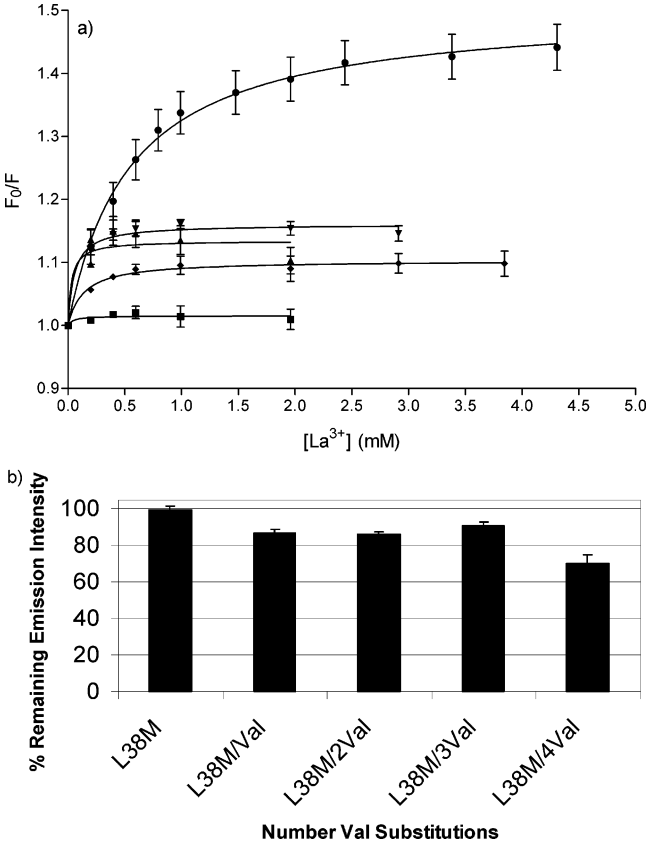

FIGURE 3: Quenching of solvent-accessible tryptophan fluorescence under nondenaturing conditions. (a) Change in emission intensity at λ_{max} during the titration of $(A\alpha_2\text{-L38M})_2$ (squares), $(A\alpha_2\text{-L38M/A8V})_2$ (triangles), $(A\alpha_2\text{-L38M/A8V/A19V})_2$ (upside-down triangles), $(A\alpha_2\text{-L38M/A8V/A19V/A44V})_2$ (diamonds), and $(A\alpha_2\text{-L38M/A8V/A19V/A44V/A55V})_2$ (circles) with 2.0 M $LaCl_3$. Data represent the mean of three replicate titrations. The error bars represent the standard deviation of the mean. (b) Percentage of original emission intensity remaining after addition of $LaCl_3$ to 1000 μL of the 2 μM four-α-helix bundle in 10 mM HEPES, pH 7.0. Tryptophan emission intensities were corrected for the dilution of the four-α-helix bundle, which occurred as a consequence of $LaCl_3$ solution addition. Maximal quenching, for a particular variant, was seen at the following $LaCl_3$ concentrations: $(A\alpha_2\text{-L38M})_2$, 1.0 mM; $(A\alpha2\text{-L38M/A8V})_2$, 2.0 mM; $(A\alpha_2\text{-L38M/A8V/A19V})_2$, 2.9 mM; $(A\alpha_2\text{-L38M/A8V/A19V/A44V})_2$, 3.8 mM; $(A\alpha_2\text{-L38M/A8V/A19V/A44V/A55V})_2$, 4.3 mM. Data represent the mean of three replicate titrations. The error bars represent the standard deviation of the mean.

$L38M)_2$ in the presence of 5.0 M Gdn-HCl (Figure 4a), indicative of an increase in the degree of solvent exposure of the tryptophan and, thus, of unfolding. For $(A\alpha_2\text{-L38M})_2$ and each variant, values for the proportion of native structure at intermediate Gdn-HCl concentrations were calculated, using the assumption that the emission λ_{max} values in 0 and 5.0 M Gdn-HCl are those of the native and maximally unfolded four-α-helix bundle, respectively (Figure 4b,c). The plots of proportion native versus [Gdn-HCl] for all variants are generally sigmoidal, suggesting that structural change in the vicinity of Trp^{15} occurs as a two-state cooperative process, although for the $(A\alpha_2\text{-L38M})_2$ bundle the data suggest that a folding intermediate may have been observed (see Discussion). The present results are thus consistent with those obtained earlier for α-helix bundles (*5*, *7*, *8*).

The reversibility of four-α-helix bundle unfolding was examined for $(A\alpha_2\text{-L38M})_2$. The curves for unfolding and refolding superimpose (Figure 4b), indicating that the unfolding of $(A\alpha_2\text{-L38M})_2$ is a reversible process. On the basis of this finding, it was assumed that the unfolding of all the $(A\alpha_2\text{-L38M})_2$ variants would be a reversible process, also.

The unfolding data for $(A\alpha_2\text{-L38M})_2$ and variants were well fit to a model for two-state reversible unfolding (*15*; Figure 4b,c). The sharpness of the transition, and therefore the cooperativity of unfolding, did, however, increase with increasing number of alanine-to-valine substitutions. This is described in a more quantitative manner in Table 1 as values for *m*. Additionally, the midpoint Gdn-HCl concentration ($[Gdn\text{-}HCl]_{mid}$) for unfolding increased as the number of alanine-to-valine substitutions was increased (Figure 4c, Table 1). This shows that the selected alanine-to-valine substitutions increase $(A\alpha_2\text{-L38M})_2$ stability and that this effect is cumulative for multiple substitutions.

The Gdn-HCl-induced unfolding of $(A\alpha_2\text{-L38M})_2$ and variants was also examined using far-UV CD spectroscopy. For $(A\alpha_2\text{-L38M})_2$, a large change in $[\theta]_{222}$ was seen in the presence of 5.0 M Gdn-HCl (Figure 5a), which is consistent with a loss of α-helical structure. Denaturation profiles were prepared by calculating values for the proportion of native four-α-helix bundles from $[\theta]_{222}$ data, which were then plotted against the corresponding [Gdn-HCl] (Figure 5b). The profiles for $(A\alpha_2\text{-L38M})_2$ and variants are all sigmoidal, which suggests that the loss of α-helical structure occurs as a two-state process, as reported previously (*5*, *7*, *8*). Circular dichroism data were also well fit to the model for two-state unfolding (Figure 5b), and the thermodynamic parameters are presented in Table 1. Like the fluorescence data, the CD

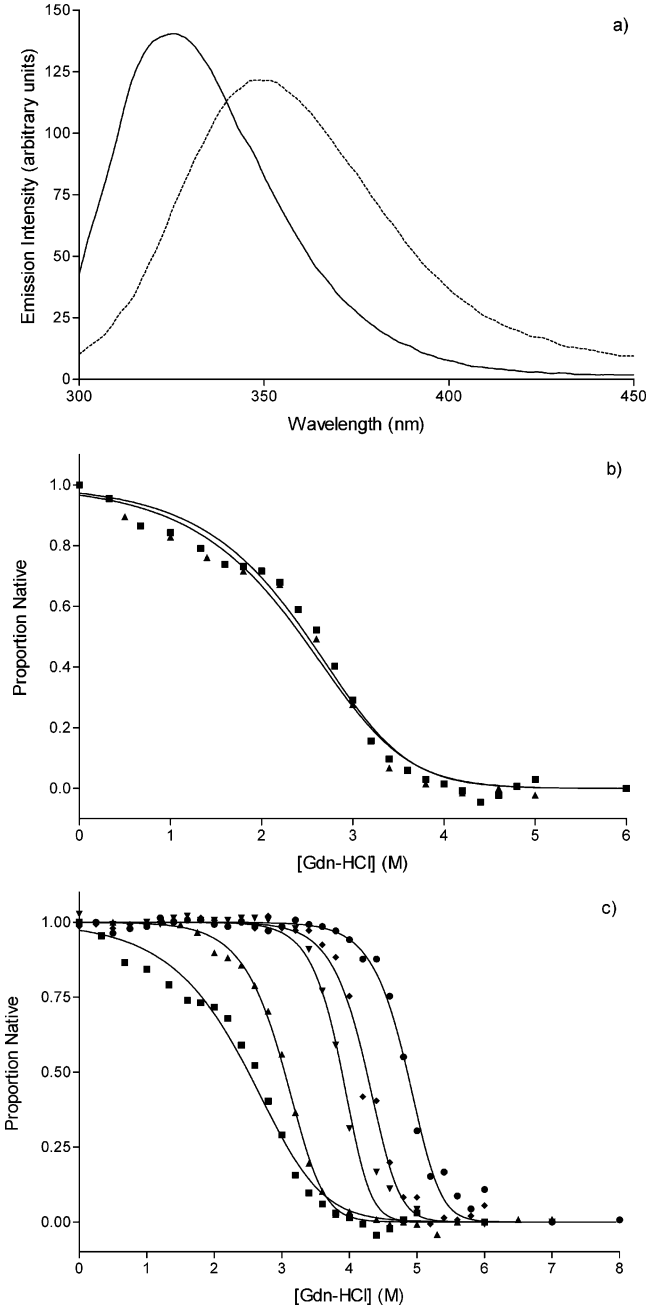

FIGURE 4: Gdn-HCl-induced unfolding of $(A\alpha_2\text{-L38M})_2$ and variants as monitored by the change in tryptophan fluorescence emission λ_{max} (2 μM four-α-helix bundle in 10 mM sodium phosphate buffer, pH 7.0). (a) Tryptophan fluorescence emission spectrum of $(A\alpha_2\text{-L38M})_2$ in the absence (—) and presence (---) of 5.0 M Gdn-HCl. (b) Unfolding profiles for $(A\alpha_2\text{-L38M})_2$ at the given concentrations of Gdn-HCl (squares) and at the given concentrations of Gdn-HCl but previously exposed to 5.0 M Gdn-HCl (triangles, to assess reversibility of unfolding). (c) Unfolding profiles for $(A\alpha_2\text{-L38M})_2$ and variants at the given [Gdn-HCl]: $(A\alpha_2\text{-L38M})_2$ (squares); $(A\alpha_2\text{-L38M/A8V})_2$ (triangles); $(A\alpha_2\text{-L38M/A8V/A19V})_2$ (upside-down triangles); $(A\alpha_2\text{-L38M/A8V/A19V/A44V})_2$ (diamonds); $(A\alpha_2\text{-L38M/A8V/A19V/A44V/A55V})_2$ (circles).

data also show that the $[\text{Gdn-HCl}]_{mid}$ for the unfolding process increased with increasing number of alanine-to-valine substitutions.

The thermodynamic parameters in Table 1 compare favorably with those obtained in earlier studies of this four-α-helix bundle (*7*). For $(A\alpha_2)_2$, for example, the ΔG^{H_2O} was

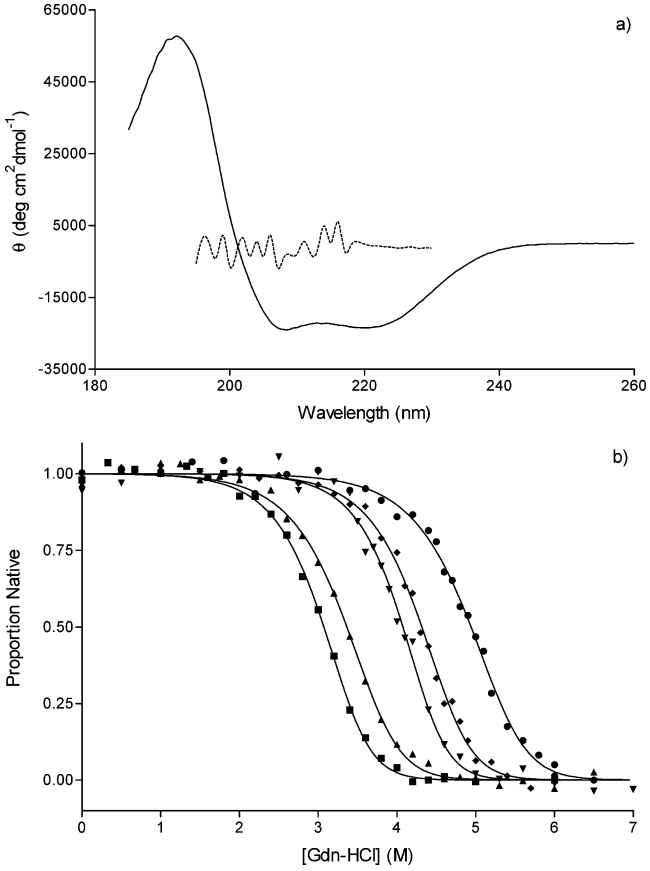

FIGURE 5: Gdn-HCl-induced unfolding of $(A\alpha_2\text{-L38M})_2$ and variants as monitored by the change in $[\theta]_{222}$ (10 μM four-α-helix bundle in 10 mM sodium phosphate buffer, pH 7.0). Concentrations of Gdn-HCl are indicated. (a) Far-UV CD spectrum of $(A\alpha_2\text{-L38M})_2$ in the absence (—) and presence (---) of 5.0 M Gdn-HCl. (b) Unfolding profiles for $(A\alpha_2\text{-L38M})_2$ (squares), $(A\alpha_2\text{-L38M/A8V})_2$ (triangles), $(A\alpha_2\text{-L38M/A8V/A19V})_2$ (upside-down triangles), $(A\alpha_2\text{-L38M/A8V/A19V/A44V})_2$ (diamonds), and $(A\alpha_2\text{-L38M/A8V/A19V/A44V/A55V})_2$ (circles).

−14.3 kcal/mol and the *m* value was 2.0 kcal/(mol M). For a redesign of Rop, $\Delta G^{H_2O} = -7.3$ kcal/mol and $m = -2.7$ kcal/(mol M) (*27*), and with 1 valine substitution, $\Delta G^{H_2O} = -8.7$ kcal/mol, 2 valine substitutions, $\Delta G^{H_2O} = -8.5$ kcal/mol, and 3 valine substitutions, $\Delta G^{H_2O} = -9.8$ kcal/mol (*28*).

Binding of Volatile Anesthetics. A titration technique was used to determine the affinities of the four-α-helix bundles for the anesthetics halothane (*4*) and chloroform (*13*). Four-α-helix bundle solution, previously equilibrated with anesthetic at a high concentration in water, and anesthetic-free four-α-helix bundle were mixed in different proportions, and the tryptophan fluorescence emission spectrum was recorded. This approach relies on the assumption that the anesthetic binds within the internal cavity of the four-α-helix bundle, where it will be retained in close proximity to the side chain of Trp^{15}, quenching its fluorescence.

Figures 6a and 7a show that, in the presence of 10 mM halothane or 35 mM chloroform, the fluorescence of $(A\alpha_2\text{-L38M})_2$ is completely quenched. This indicates an interaction between Trp^{15} and the anesthetic, which occurs when $(A\alpha_2\text{-L38M})_2$ binds anesthetic as described above. The titration curves for $(A\alpha_2\text{-L38M})_2$ are shown in Figures 6b and 7b.

Two control titrations were carried out to substantiate the claim that halothane and chloroform bind in the internal cavity of the four-α-helix bundles. In the first control study,

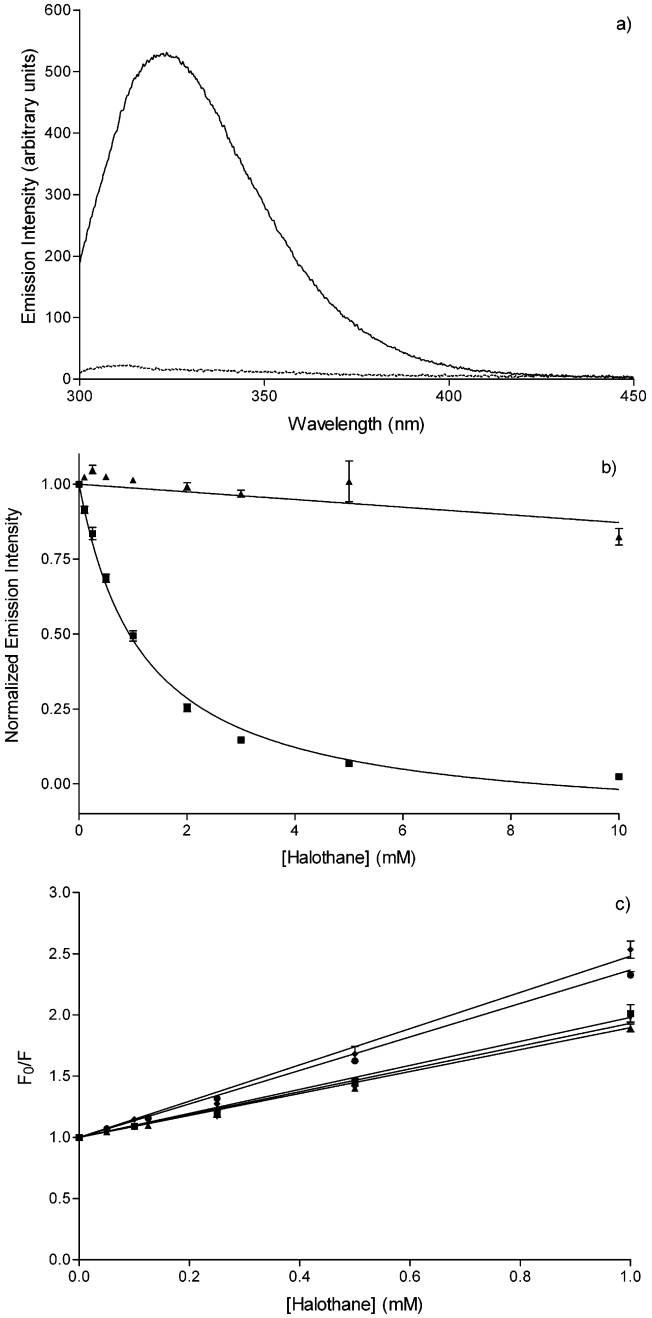

FIGURE 6: Binding of halothane to $(A\alpha_2\text{-L38M})_2$ and variants as monitored by the gradual quenching of tryptophan fluorescence in 20 mM sodium phosphate buffer and 130 mM NaCl, pH 7.0. The four-α-helix bundle concentration was 2 μM. (a) Tryptophan emission spectrum of $(A\alpha_2\text{-L38M})_2$ in buffer in the absence (—) and in the presence (---) of 10 mM halothane. (b) Titration of $(A\alpha_2\text{-L38M})_2$ with halothane in the presence (triangles) and absence (squares) of 5.0 M Gdn-HCl. (c) Stern−Volmer plots for the titration of $(A\alpha_2\text{-L38M})_2$ (squares), $(A\alpha_2\text{-L38M/A8V})_2$ (triangles), $(A\alpha_2\text{-L38M/A8V/A19V})_2$ (upside-down triangles), $(A\alpha_2\text{-L38M/A8V/A19V/A44V})_2$ (diamonds), and $(A\alpha_2\text{-L38M/A8V/A19V/A44V/A55V})_2$ (circles) with halothane. Data represent the mean of three replicate titrations. The error bars represent the standard deviation of the mean.

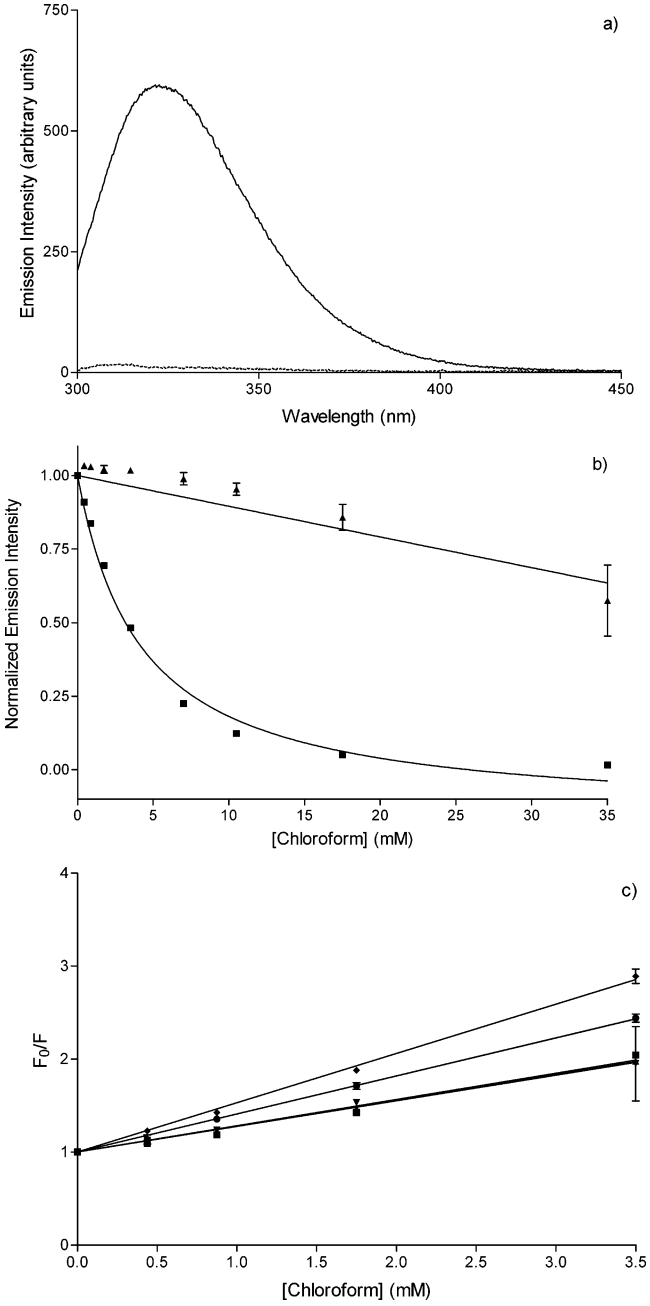

FIGURE 7: Binding of chloroform to $(A\alpha_2\text{-L38M})_2$ and variants as monitored by the gradual quenching of tryptophan fluorescence in 20 mM sodium phosphate buffer and 130 mM NaCl, pH 7.0. The four-α-helix bundle concentration was 2 μM. (a) Tryptophan emission spectrum of $(A\alpha_2\text{-L38M})_2$ in buffer in the absence (—) and in the presence (---) of 35 mM chloroform. (b) Titration of $(A\alpha_2\text{-L38M})_2$ with chloroform in the presence (triangles) and absence (squares) of 5.0 M Gdn-HCl. (c) Stern−Volmer plots for the titration of $(A\alpha_2\text{-L38M})_2$ (squares), $(A\alpha_2\text{-L38M/A8V})_2$ (triangles), $(A\alpha_2\text{-L38M/A8V/A19V})_2$ (upside-down triangles), $(A\alpha_2\text{-L38M/A8V/A19V/A44V})_2$ (diamonds), and $(A\alpha_2\text{-L38M/A8V/A19V/A44V/A55V})_2$ (circles) with chloroform. Data represent the mean of three replicate titrations. The error bars represent the standard deviation of the mean.

$(A\alpha_2\text{-L38M})_2$ in 5.0 M Gdn-HCl was titrated with halothane and chloroform, and the decrease in tryptophan emission intensity was followed. Figure 6b shows that the maximum extent of quenching by halothane is approximately 12-fold less in the presence of 5.0 M Gdn-HCl than in its absence. For the analogous chloroform titrations, a similar decrease in the maximum extent of quenching was observed (Figure 7b). In 5.0 M Gdn-HCl, the four-α-helix bundle is unfolded, the anesthetic binding site is lost, and the side chain of Trp^{15} is solvent-exposed. Therefore, the diminished tryptophan fluorescence quenching observed in the presence of 5.0 M Gdn-HCl is consistent with fluorescence quenching by an aqueous collisional mechanism only.

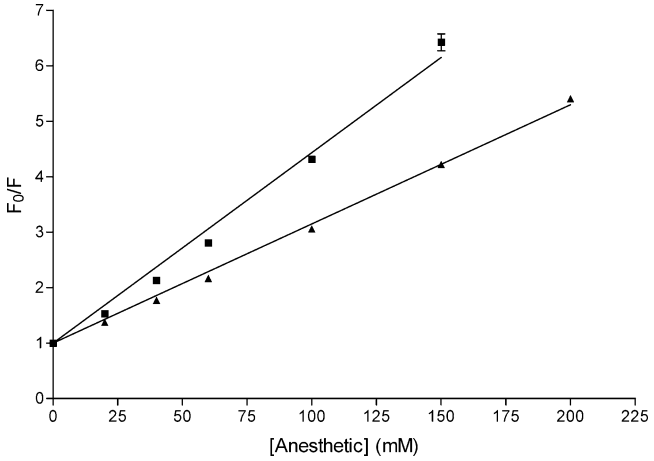

FIGURE 8: Stern−Volmer plots for the interaction of NATA with halothane (squares, $K_{SV} = 0.03\ M^{-1}$) and chloroform (triangles, $K_{SV} = 0.02\ M^{-1}$) in methanol. Values for K_{SV} were determined by fitting the data to the equation $F_0/F = 1 + K_{SV}$[anesthetic], where K_{SV} = slope, F_0 is the unquenched fluorescence intensity, and F is the fluorescence intensity at a given anesthetic concentration (*41*). Data represent the mean of three replicate titrations. The error bars represent the standard deviation of the mean.

Table 2: Parameters for the Binding of Halothane and Chloroform to $(A\alpha_2\text{-L38M})_2$ Four-α-Helix Bundles

four-α-helix bundle	anesthetic K_d (mM)[a]	anesthetic K_{SV} (mM^{-1})[a]
$(A\alpha_2\text{-L38M})_2$	1.0 ± 0.1	1.0
	3.5 ± 0.6	*0.3*
$(A\alpha_2\text{-L38M/Val})_2$	1.1 ± 0.1	0.9
	3.6 ± 0.2	*0.3*
$(A\alpha_2\text{-L38M/2Val})_2$	1.1 ± 0.1	0.9
	3.6 ± 0.4	*0.3*
$(A\alpha_2\text{-L38M/3Val})_2$	0.7 ± 0.1	1.5
	1.9 ± 0.2	*0.5*
$(A\alpha_2\text{-L38M/4Val})_2$	0.7 ± 0.1	1.4
	2.4 ± 0.3	*0.4*
$(A\alpha_2\text{-L38M})_2$ in 5.0 M Gdn-HCl		0.02
		0.02
NATA		0.03
		0.02

[a] Roman type for halothane values. Italic type for chloroform values.

A second control study was made to validate the interpretation of the data collected for $(A\alpha_2\text{-L38M})_2$ in 5.0 M Gdn-HCl (Figures 6b and 7b). *N*-Acetyltryptophanamide (NATA) was titrated with halothane and chloroform (Figure 8), and the results obtained were compared with those for $(A\alpha_2\text{-L38M})_2$ collected in 5.0 M Gdn-HCl. It was, however, necessary to collect the NATA data in methanol due to the low aqueous solubility of both the fluorophore and anesthetics. *N*-Acetyltryptophanamide was selected for this control study because it is a small molecule and fluorescence quenching can only occur via a collisional mechanism. It is therefore reasonable to assume that the collision-only mechanism for this fluorescence quenching phenomenon should give similar Stern−Volmer plots to those for the quenching of the solvent-exposed tryptophan side chains of $(A\alpha_2\text{-L38M})_2$ in 5.0 M Gdn-HCl by halothane and chloroform. Thus, the observed similarity in K_{SV} values (Table 2) for the titration of anesthetics with NATA and $(A\alpha_2\text{-L38M})_2$ in 5.0 M Gdn-HCl suggests that collisional quenching is indeed the predominant mechanism by which $(A\alpha_2\text{-L38M})_2$ tryptophan fluorescence is quenched in the presence of 5.0 M Gdn-HCl. This, in turn, substantiates the claim that the stronger quenching seen when these four-α-helix bundles are titrated in the absence of Gdn-HCl is due to the binding of halothane and chloroform within the internal cavity. Furthermore, after having subtracted the collisional quenching component from these four-α-helix bundle data, it is reasonable to assume that K_{SV} values are the reciprocol of K_d values. Thus, any observed differences in anesthetic binding affinities among the variants should therefore reflect the differing number of valine side chains in the internal cavity of the four-α-helix bundle.

Stern−Volmer plots were used to compare the binding affinities of $(A\alpha_2\text{-L38M})_2$ and variants for halothane and chloroform (Figures 6c and 7c). They show that the affinities of $(A\alpha_2\text{-L38M})_2$, $(A\alpha_2\text{-L38M/A8V})_2$, and $(A\alpha_2\text{-L38M/A8V/A19V})_2$ for halothane are similar. The same is true for the affinities of these variants for chloroform. However, both halothane and chloroform are bound more tightly to $(A\alpha_2\text{-L38M/A8V/A19V/A44V/A55V})_2$ and $(A\alpha_2\text{-L38M/A8V/A19V/A44V})_2$ (Figures 6c and 7c, Table 2).

DISCUSSION

The aims of the present study were to investigate how alanine-to-valine substitutions in the internal cavity of a four-α-helix bundle affected structure, stability, and anesthetic binding affinity. It was hoped that in making these substitutions the binding affinities of halothane and chloroform for $(A\alpha_2\text{-L38M})_2$ would be increased. None of the substitutions investigated here had any appreciable effect on the proportion of α-helix in $(A\alpha_2\text{-L38M})_2$; values ranged from 73.4% to 77.8% (Table 1). The substitutions did, however, effect the environment of Trp^{15} and thus tertiary structure in the vicinity of this side chain. The extent of fluorescence quenching of solvent-exposed tryptophan side chains by La^{3+} showed a modest increase with increasing number of alanine-to-valine substitutions. Thus, it appears that the selected valine substitutions force the side chain of Trp^{15} into a more solvent-exposed environment. This suggests that, in the vicinity of Trp^{15} at least, the four-α-helix bundle structure is more open and expanded. The larger side chain of valine may introduce steric strain into the four-α-helix bundle structure, forcing the α-helices apart.

It has been reported earlier that protein tertiary structures can accommodate some amino acid substitutions with only minor changes in secondary structure. For similar types of substitutions in T4 lysosyme, for example, the polypeptide backbone usually shifts between 0.25 and 0.5 Å to compensate for the change in side chain volume (*29*−*32*). A more extensive shuffling of tertiary structure may, however, be necessary, with side chain shifts of between 1 and 2 Å being reported in T4 lysosyme, for example. Some mutations may also lead to a small expansion of the entire molecule (*30*).

The alanine-to-valine substitutions had an appreciable effect on the stability of $(A\alpha_2\text{-L38M})_2$. For each substitution the $[Gdn\text{-}HCl]_{mid}$ increased by between 0.3 and 0.8 M (Table 1). Values for ΔG^{H_2O} also show a general increase with increasing number of substitutions, although the trend is not as well defined as that for $[Gdn\text{-}HCl]_{mid}$. The selected substitutions probably stabilize $(A\alpha_2\text{-L38M})_2$ through entropic effects. The ΔS for the transfer of a side chain from the protein interior to the solvent will be more unfavorable for valine than for alanine.

The CD results in Figure 5 and Table 1 show two discrete "magnitudes" to the increase in $[Gdn\text{-}HCl]_{mid}$ resulting from the selected alanine-to-valine substitutions. When going from zero to one and from two to three substitutions, $[Gdn\text{-}HCl]_{mid}$ increased by approximately 0.3 M. When going from one to two and from three to four substitutions, $[Gdn\text{-}HCl]_{mid}$ increased by approximately 0.7 M. This grouping may reflect the position in the heptad repeat where the substitutions are made. The increases of 0.3 M occur as a consequence of substitutions at position a, while the increases of 0.7 M occurred for substitutions at position d. An earlier report (*33*) states that, in a coiled coil, side chains at heptad position a point into the hydrophobic core less than those at position d. Consistent with this observation, the larger increases in $[Gdn\text{-}HCl]_{mid}$ for $(A\alpha_2\text{-}L38M)_2$ occur as a consequence of the substitutions at position d.

For variants with zero and one alanine-to-valine substitution in particular, the $[Gdn\text{-}HCl]_{mid}$ values determined from fluorescence data are less than those determined from CD data (Figure 5b, Table 1). This suggests that, during the unfolding of these variants, a structural change in the vicinity of Trp^{15}, which leads to a modest increase in the solvent exposure of this side chain, precedes a global structural change in the amount of α-helix. Thus, $(A\alpha_2\text{-}L38M)_2$ and $(A\alpha_2\text{-}L38M/A8V)_2$ in particular appear to unfold via a molten globule-like intermediate. For $(A\alpha_2\text{-}L38M/A8V/A19V)_2$, $(A\alpha_2\text{-}L38M/A8V/A19V/A44V)_2$, and $(A\alpha_2\text{-}L38M/A8V/A19V/A44V/A55V)_2$, where $[Gdn\text{-}HCl]_{mid}$ and ΔG^{H_2O} values determined from CD and fluorescence data show a greater similarity, there is less evidence for the formation of an unfolding intermediate. The fluorescence data for these variants in the native state may hold the key to why this is. Fluorescence quenching by La^{3+} shows that the proportion of solvent-exposed tryptophan side chains is greater for those variants with more valine residues. Therefore, because the valine-rich variants appear to have a slightly more open structure under benign conditions, they may already be in the molten globule-like state $(A\alpha_2\text{-}L38M)_2$ and $(A\alpha_2\text{-}L38M/A8V)_2$ move through when they are unfolded. The fluorescence data in Figure 4 also support the notion that an intermediate exists on the unfolding pathway of $(A\alpha_2\text{-}L38M)_2$ and $(A\alpha_2\text{-}L38M/A8V)_2$ in particular. The slopes in the region of the unfolding transition are less for these variants than for the more highly substituted ones. Thus, the values for *m* (Table 1) are lowest for $(A\alpha_2\text{-}L38M)_2$ and $(A\alpha_2\text{-}L38M/A8V)_2$, suggesting that they unfold in the least cooperative manner of the variants examined here.

The existence of an intermediate on the folding/unfolding pathway of four-α-helix bundles from the $(A\alpha_2)_2$ family has been reported earlier (*34*). It was shown that, for equilibrium unfolding in Gdn-HCl, the midpoint concentrations measured by far-UV CD differed from those measured by tryptophan fluorescence. Additonally, in 6.0 M Gdn-HCl the fluorescence λ_{max} was red shifted relative to that at high pressure (i.e., 3.5 kbar) or at low temperature (i.e., 0−5 °C). From these results it was concluded that at moderate Gdn-HCl concentrations (i.e., <2.5 M), at high pressure and at low temperature, $(A\alpha_2)_2$ assumes a dissociated molten globule-like state (*34*).

The variation in binding affinities discussed above follows a clear trend. $(A\alpha_2\text{-}L38M)_2$, $(A\alpha_2\text{-}L38M/A8V)_2$, and $(A\alpha_2\text{-}L38M/A8V/A19V)_2$ bind halothane with similar affinities (K_d approximately 1.0 ± 0.1 mM**)**, while $(A\alpha_2\text{-}L38M/A8V/A19V/A44V)_2$ and $(A\alpha_2\text{-}L38M/A8V/A19V/A44V/A55V)_2$ bind this ligand more tightly (K_d = 0.7 ± 0.1 mM; Table 2). The same trend in binding affinities was seen for the corresponding set of titrations made using chloroform, although for a particular variant, the K_d values for this anesthetic indicated weaker binding: $(A\alpha_2\text{-}L38M)_2$, $(A\alpha_2\text{-}L38M/A8V)_2$, and $(A\alpha_2\text{-}L38M/A8V/A19V)_2$ bound chloroform with a K_d of 3.5 ± 0.6 mM, while $(A\alpha_2\text{-}L38M/A8V/A19V/A44V)_2$ and $(A\alpha_2\text{-}L38M/A8V/A19V/A44V/A55V)_2$ bound chloroform with an average K_d of 2.1 ± 0.3 mM (Table 2). Thus, it appears that the internal binding cavity of $(A\alpha_2\text{-}L38M)_2$ is optimized for anesthetic binding when the substitutions A8V, A19V, A44V, and A55V are made; increasing the number of valine side chains in the internal cavity of $(A\alpha_2\text{-}L38M)_2$ improves the shape complementarity between anesthetic and binding site. For this anesthetic/four-α-helix bundle combination the forces and interactions which favor binding include the favorable ΔS associated with the removal of the hydrophobic anesthetic molecules from the solvent and perhaps the removal of any polar solvent molecules previously bound in the hydrophobic cavity of the four-α-helix bundle. Forces that stabilize the anesthetic/four-α-helix bundle complex will also include the ΔH associated with the formation of specific interactions between groups on the ligand and groups in the four-α-helix bundle internal cavity. In contrast, the ΔS associated with constraining the ligand in the binding site, which will result in a loss of rotational and translational freedom, will disfavor anesthetic binding. However, this effect will be offset to the greatest extent in the case of the interactions of anesthetic with $(A\alpha_2\text{-}L38M/A8V/A19V/A44V)_2$ and $(A\alpha_2\text{-}L38M/A8V/A19V/A44V/A55V)_2$.

The results obtained in the present study are consistent with those of earlier studies in which the binding of hydrophobic ligands to mutants of T4 lysosyme was investigated (*35*, *36*). Initially, it was determined that the L99A mutant was capable of binding benzene with a K_a of 5.7 mM^{-1} (*35*, *36*). Following from this, the nature of the binding site of this mutant was further characterized by measuring the binding affinities of phenylalkanes of increasing alkyl chain length (*35*). It was found that binding to L99A became progressively tighter, up to an alkyl chain length of four carbons: K_a(toluene) = 9.8 mM^{-1}, K_a(ethylbenzene) = 14.8 mM^{-1}, K_a(propylbenzene) = 55.2 mM^{-1}, and K_a(*n*-butylbenzene) = 69.8 mM^{-1}. In the present study the size and hydrophobicity of the ligand were held constant while those of the binding site on the protein were varied. When either three or four alanine side chains were changed to valine, the binding affinity of halothane and chloroform increased approximately 2-fold. This is consistent with the earlier results (*35*), where ethylbenzene and *n*-butylbenzene were found to bind approximately 3 times and 12 times as tightly as benzene, respectively. Thus, in the case of $(A\alpha_2\text{-}L38M)_2$ in particular, it appears that an alteration in the size and hydrophobicity of the ligand binding site does not have a dramatic effect on ligand binding affinity. Previously, it was also suggested that α-helices can shift to accommodate ligands (*37*). This may be true up to a point for $(A\alpha_2\text{-}L38M)_2$.

For all five variants examined here, chloroform has K_d values that are consistent with weaker binding compared with halothane. This may reflect three phenomena. First, the

somewhat larger halothane (123 Å^3; *13*) may fit the binding site more optimally than the smaller chloroform (102 Å^3; *38*). The larger halothane may thus be maintained for longer periods of time in an orientation that permits more efficient quenching of tryptophan fluorescence. Second, chloroform is less polarizable than halothane since it lacks the bromine atom, and therefore the dipole/induced dipole (Debye) and induced dipole/induced dipole (London) forces that are formed as a consequence of binding to the four-α-helix bundles will be weaker. Third, the permanent dipole moment of halothane (2.18 D; *39*) is greater than that of chloroform (1.15 D; *40*), allowing for stronger dipole/induced dipole interactions in the binding site. In addition to these effects, the NATA control data (Figure 8) show that the degree of fluorescence quenching seen with chloroform is less than that seen with halothane. This suggests that chloroform is a less efficient quencher of tryptophan fluorescence than halothane. Although this will not affect the calculated values for K_d, it will affect values for Q_{max}, the extent of quenching seen at infinite anesthetic concentration.

The K_d value for the binding of halothane to $(A\alpha_2\text{-L38M})_2$ reported in ref *7* is 200 μM, while the value reported here for this system is 1.0 mM (Table 2). We attribute this discrepancy to the different batches of purified $(A\alpha_2\text{-L38M})_2$ used in these two studies.

Because the study presented here addresses the binding of hydrophobic anesthetics to water-soluble receptors, it is acknowledged that discrepancies between this system and the in vivo system, where the receptors are embedded in cell membranes, exist. For example, the α-helix bundles of membrane-bound proteins can be distorted and twisted (*3*). Thus, the shapes of the internal cavities of such receptors may differ somewhat from those of the water-soluble four-α-helix bundles examined here. This, in turn, may affect anesthetic binding affinities. Additionally, the hydrophobic anesthetics examined in this study will not partition between receptor and solution (as examined here) in the same way as they would between receptor and lipid (as would be the case in vivo). For this reason also, the anesthetic binding affinities measured and discussed here may differ from the true in vivo affinities. However, the use of our synthetic water-soluble four-α-helix bundles to study anesthetic/receptor interactions is of appreciable interest; the K_d values for halothane discussed here are very similar to the in vivo EC_{50} values for this anesthetic (see the introduction).

The results from the present study further our understanding of the structure of the in vivo receptors of inhalational anesthetics. From earlier studies it was determined that having a flexible methionine side chain in the binding cavity of the four-α-helix bundle of $(A\alpha_2)_2$ improves ligand binding affinity (*7*). Additionally, it has been suggested that dipole (i.e., from anesthetic)/aromatic quadrupole (i.e., from binding site) interactions are involved in ligand binding (*8*). Finally, the present results offer insight into the optimal volume of the ligand/anesthetic binding cavity of $(A\alpha_2)_2$-type four-α-helix bundles. Those variants with zero, one, and two substitutions bound halothane with similar affinities. The same was true for the binding of chloroform to these variants. $(A\alpha_2\text{-L38M/A8V/A19V/A44V})_2$ and $(A\alpha_2\text{-L38M/A8V/A19V/A44V/A55V})_2$, however, bound both anesthetics more tightly. This suggests that the anesthetic/binding cavity shape complementarity is optimized in the $(A\alpha_2\text{-L38M})_2$ variant with three and four additional valines in the internal cavity. Efforts are currently being made to obtain crystal structures of the four-α-helix bundles discussed here in order to gain a more detailed understanding of how inhalational anesthetics bind to their receptor proteins in vivo.

The effects of the selected alanine-to-valine substitutions on $(A\alpha_2\text{-L38M})_2$ structure and stability were also examined here. None of the substitutions have any appreciable effect on the amount of secondary structure in this four-α-helix bundle. However, it appears that the overall structure of $(A\alpha_2\text{-L38M})_2$ becomes slightly more open as a consequence of multiple alanine-to-valine substitutions. This is reflected in an increase in the ability of the La^{3+} to quench the fluorescence from the tryptophan side chain.

Finally, alanine-to-valine substitutions stabilize the native structure of $(A\alpha_2\text{-L38M})_2$ toward unfolding, and this effect is cumulative for multiple substitutions, with unfolding becoming more cooperative as the number of valine residues is increased.

ACKNOWLEDGMENT

Mass spectrometry analyses were performed by the Protein Chemistry Laboratory, University of Pennsylvania, Philadelphia, PA.

REFERENCES

1. Franks, N. P., and Lieb, W. R. (1994) Molecular and cellular mechanisms of general anesthesia, *Nature 367*, 607−614.
2. Harris, R. A., Mihic, S. J., Dildy-Mayfield, J. E., and Machu, T. K. (1995) Actions of anesthetics on ligand-gated ion channels: role of receptor subunit composition, *FASEB J. 9*, 1454−1462.
3. Doyle, D. A., Cabral, J. M., Pfuetzner, R. A., Kuo, A., Gulbis, J. M., Cohen, S. L., Chait B. T., and MacKinnon, R. (1998) The structure of the potassium channel: molecular basis for K^+ conduction and selectivity, *Science 280*, 69−70.
4. Johansson, J. S., Rabanal, F., and Dutton, P. L. (1996) Binding of the volatile anesthetic halothane to the hydrophobic core of a tetra-α-helix bundle protein, *Pharmacol. Exp. Ther. 279*, 56−61.
5. Johansson, J. S., Gibney, B. R., Skalicky, J. J., Wand, A. J., and Dutton, P. L. (1998) A designed cavity in the hydrophobic core of a four-a-helix bundle improves volatile anesthetic binding affinity, *Biochemistry 37*, 1421−1429.
6. Johansson, J. S., Gibney, B. R., Skalicky, J. J., Wand, A. J., and Dutton, P. L. (1998) A native-like three-α-helix bundle protein from structure based redesign: a novel maquette scaffold, *J. Am. Chem. Soc. 120*, 3881−3886.
7. Johansson, J. S., Scharf, D., Davies, L. A., Reddy, K. S., and Eckenhoff, R. G. (2000) A designed four-α-helix bundle that binds the volatile general anesthetic halothane with high affinity, *Biophys. J. 78*, 982−993.
8. Manderson, G. A., and Johansson, J. S. (2002) Role of aromatic side-chains in the binding of volatile general anesthetics to a four-α-helix bundle, *Biochemistry 41*, 4080−4087.
9. Pokutta, S., Drees, F., Takai, Y., Nelson, W. J., and Weis, W. I. (2002) Biochemical and structural definition of the l-afadin- and actin-binding sites of α-catenin, *J. Biol. Chem. 277*, 18868−18874.
10. Liu, G., Guibao, C. D., and Zheng, J. (2002) Structural insight into the mechanisms of targeting and signaling of focal adhesion kinase, *Mol. Cell. Biol. 22*, 2751−2760.
11. Wassner, A. J., Hurt, J. A., Lear, J. D., and Akerfeldt, K. S. (2002) Synthesis and ion conductance behavior of a tetrameric alamethicin ion channel, *Org. Lett. 4*, 1647−1649.
12. Lakowicz, J. R. (1983) in *Principles of Fluorescence Spectroscopy*, p 354, Plenum Publishing Corp., New York, NY.
13. Johansson, J. S., Solt, K., and Reddy, K. S. (2003) Binding of the general anesthetics chloroform and 2,2,2-trichloroethanol to the hydrophobic core of a four-α-helix bindle protein, *Photochem. Photobiol. 77*, 20−26.
14. Shibata, A., Morita, K., Yamashita, T., Kamaya, H., and Ueda, I. (1991) Anesthetic-protein interaction: effects of volatile anesthet-

ics on the secondary structure of poly(L-lysine), *J. Pharm. Sci. 80*, 1037−1041.
15. Starna (1980) Reference materials for molecular fluorescence spectrophotometry, Starna, Hainault, Essex IG6 3UT, England.
16. Mok, Y.-K., De Prat Gay, G., Butler, J. P., and Bycroft, M. (1996) Equilibrium dissociation and unfolding of the dimeric human papillomavirus strain-16 E2 DNA-binding domain, *Protein Sci. 5*, 310−319.
17. Bastyns, K., and Engelborghs, Y. (1992) Acrylamide quenching of the fluorescence of glyceraldehydes-3-phosphate dehydrogenase: reversible and irreversible effects, *Photochem. Photobiol. 55*, 9−16.
18. Brahms, S., and Brahms, J. (1980) Determination of protein secondary structure in solution by vacuum ultraviolet circular dichroism, *J. Mol. Biol., 138*, 149−178.
19. Chan, Y.-H., Yand, J. T., and Chau, K. H. (1974) Determination of the helix and beta form of proteins in aqueous solution by circular dichroism, *Biochemistry 13*, 3350−3359.
20. Walsh, S. T. R., Cheng, H., Bryson, J. W., Roder, H., and DeGrado, W. F. (1999) Solution structure and dynamics of a *de novo* designed three-helix bundle protein, *Proc. Natl Acad. Sci. U.S.A. 96*, 5486−5491.
21. Takano, N. (1977) Structure of myoglobin refined at 2.0 Å resolution, *J. Mol. Biol. 110*, 569−584.
22. LaBrake, C. C., Wang, L., Keiderling, T. A., and Fung, L. W.-M. (1993) Fourier transform infrared spectroscopic studies of the secondary structure of spectrin under different ionic strengths, *Biochemistry 32*, 10296−10302.
23. O'Neil, K. T., and DeGrado, W. F. (1990) A thermodynamic scale for the helix-forming tendencies of the commonly occurring amino acids, *Science 250*, 646−651.
24. Eftink, M. R., and Ghiron, C. (1981) Fluorescence quenching studies with proteins, *Anal. Biochem. 114*, 199−227.
25. Lau, S. Y. M., Taneja, A. K., and Hodges, R. S. (1984) Synthesis of a model protein of defined secondary and quaternary structure. Effect of chain length on the stabilization and formation of two-stranded alpha-helical coiled-coils, *J. Biol. Chem. 259*, 13253−13261.
26. Cooper, T. M., and Woody, R. W. (1990) The effect of conformation on the CD of interacting helices: a theoretical study of tropomyosin, *Biopolymers 30*, 657−676.
27. Munson, M., O'Brien, R., Sturtevant, J. M., and Regan, L. (1994) Redesigning the hydrophobic core of a four-helix-bundle protein, *Protein Sci. 3*, 2015−2022.
28. Betz, S. F., Liebman, P. A., and DeGrado, W. F. (1997) *De novo* design of native proteins: characterization of proteins intended to fold into antiparallel, rop-like, four-helix bundles, *Biochemistry 36*, 2450−2458.
29. Anderson, D. E., Hurley, J. H., Nicholson, H., Baase, W. A., and Matthews, B. W. (1993) Hydrophobic core repacking and aromatic−aromatic interaction in the thermostable mutant of T4 lysozyme Ser 117→Phe, *Protein Sci. 2*, 1285−1290.
30. Baldwin, E. P., and Matthews, B. W. (1994) Core-packing constraints, hydrophobicity and protein design, *Curr. Opin. Biotechnol. 5*, 396−402.
31. Xu, J., Baase, W. A., Baldwin, E., and Matthews, B. (1998) The response of T4 lysozyme to large-to-small substitutions within the core and its relation to the hydrophobic effect, *Protein Sci. 7*, 158−177.
32. Baldwin, E. P., and Matthews, B. W. (1994) Core-packing constraints, hydrophobicity and protein design, *Curr. Opin. Biotechnol. 5*, 396−402.
33. Tripet, B., Wagschal, K., Lavigne, P., Mant, C. T., and Hodges, R. S. (2000) Effects of side-chain characteristics on stability and oligomerization state of a de novo-designed model coiled-coil: 20 amino acid substitutions in position "d", *J. Mol. Biol. 300*, 377−402.
34. Chapeaurouge, A., Johansson, J. S., and Ferreira, S. T. (2002) Folding of a de novo designed nativelike four-helix bundle protein, *J. Biol. Chem. 277*, 16478−16483.
35. Morton, A., Baase, W. A., and Matthews, B. W. (1995) Energetic origins of specificity of ligand binding in an interior nonpolar cavity of T4 lysozyme, *Biochemistry 34*, 8564−8575.
36. Baldwin, E., Baase, W. A., Zhang, X−j., Feher, V., and Matthews, B. W. (1998) Generation of ligand binding sites in T4 lysozyme by deficiency-creating substitutions, *J. Mol. Biol. 277*, 467−485.
37. Blaber, M., Lindstrom, J. D., Gassner, N., Xu, J., Heinz, D. W., and Matthews, B. W. (1993) Energetic cost and structural consequences of burying a hydroxyl group within the core of a protein determined from Ala→Ser and Val→Thr substitutions in T4 lysozyme, *Biochemistry 32*, 11363−11373.
38. Abraham, M. H., and McGowan, J. C. (1987) The use of characteristic volumes to measure cavity terms in reversed phase liquid chromatography, *Chromatographia 23*, 243−246.
39. Scharf, D., and Laasonen, K. (1993) Structure, effective pair potential and properties of halothane, *Chem. Phys. Lett. 258*, 276−282.
40. Raines, D. E., and Claycomb, R. J. (2002) The role of electrostatic interactions in governing anesthetic action on the torpedo nicotinic acetylcholine receptor, *Anesth. Analg. 95*, 356−361.
41. Ueda, I., and Kamaya, H. (1973) Kinetic and thermodynamic aspects of the mechanism of general anesthesia in a model system of firefly luminescence in vitro, *Anesthesiology 38*, 425−436.

BI034623B